DOI: 10.1002/anie.201101783

Cancer Therapeutics

Multifunctional Nanoparticles for Targeted Chemophotothermal Treatment of Cancer Cells**

*Sun-Mi Lee, Huiyul Park, Joung-Woo Choi, Young Nyun Park, Chae-Ok Yun, and Kyung-Hwa Yoo**

Despite remarkable progress in cancer therapeutics, substantial impediments are still unresolved, such as severe adverse reactions and poor effectiveness against multidrug-resistant cancer cells. Most anticancer drugs exhibit high efficacy with a variety of solid tumors; however, nonspecific delivery leads to substantial toxicity to normal tissue and limits dosages of anticancer drugs to levels far below those required to destroy the tumor completely. To overcome these problems, various targeted drug deliveries and combined treatments to enhance the cytotoxic effect of anticancer drugs have been investigated. Regarding targeted delivery, molecular ligands such as antibodies, peptides, or small molecules have been used to recognize specific receptors on the surface of the tumor cell; various liposomes and nanomaterials conjugated with targeting ligands have been shown to achieve targeted delivery.[1] One combined treatment with chemotherapy is thermochemotherapy. Heat treatment resonant nanomaterials[3,4] have been reported to be superior to chemotherapy or photothermal treatment alone. Thus far, combinations of chemotherapy with hyperthermia and targeted delivery have been explored independently. However, were chemotherapy combined with both hyperthermia and targeted delivery, a higher therapeutic efficacy would be achieved by this triple combination in comparison with the pairwise combinations. In particular, if therapeutic antibodies were used as targeting ligands to specifically target the tumor cells and stimulate the immune system to attack them, simultaneous and efficient delivery of the targeting ligands, drug, and heat to the tumor would improve therapeutic efficacy and minimize side effects.

To combine chemotherapy with hyperthermia and targeted delivery, we developed doxorubicin-loaded poly(ethylene glycol)–poly(lactic-*co*-glycolic acid)–Au half-shell nanoparticles (DOX-PLGA-Au H-S NPs) and conjugated anti-human epidermal growth factor receptor 2 (HER2) antibodies, Herceptin (HER), to the surface of the Au half-shell. On NIR irradiation, heat is locally generated due to NIR resonance of the Au half-shells, and DOX release from PLGA-Au H-S NPs is accelerated.[4] In addition, conjugated HER allows these nanoparticles to be specifically delivered to HER2 overexpressed from a breast cancer cell line (SK-BR-3) in a mouse model and to be internalized by receptor-mediated endocytosis.[5] As a result, the total accumulation of nanoparticles is enhanced in the targeted tumor, and heat, drug, and therapeutic antibodies are simultaneously delivered to the selected tumor region with a laser-guided light source. Here, we report the use of HER-conjugated DOX-PLGA-Au H-S NPs in a tumor-bearing mouse. With these nanoparticles and NIR irradiation, complete tumor destruction without recurrence was induced by lower DOX dosages compared to chemophotothermal treatment without HER or targeted drug delivery without NIR irradiation. Moreover, since the administered DOX dosage was too low to cause normal-tissue toxicity, substantial side effects were not observed.

We prepared four different kinds of nanoparticles (Figure 1 a): PLGA-Au H-S NPs, HER-conjugated PLGA-Au H-S NPs (HER-PLGA-Au H-S NPs), DOX-loaded PLGA-Au H-S NPs (DOX-PLGA-Au H-S NPs), and HER-conjugated/DOX-loaded PEG-PLGA-Au H-S NPs (HER-DOX-PLGA-Au H-S NPs). First, PLGA NPs with and without DOX were synthesized as previously reported.[4] Then, Au (15 nm) was deposited onto an NP monolayer prepared on an Si substrate with a thermal evaporator, followed by functionalization of the Au surface with thiol-terminated methoxy-PEG to improve the NP stability under physiological conditions (PLGA-Au H-S NPs and DOX-PLGA-Au H-S NPs). For targeted delivery, HER was conjugated on the Au surface by using protein G as linker (HER-PLGA-Au H-S NPs and HER-DOX-PLGA-Au H-S NPs).

In UV/Vis/NIR absorption spectra, all specimens exhibited a pronounced peak at approximately 800 nm due to the Au half-shell (Figure 1 b), which suggests that NIR irradiation leads to photothermal conversion effects for all samples. To investigate the targeting efficacy of HER-PLGA-Au H-S NPs, we incubated SK-BR-3 cancer cells expressing high levels of HER2 with PLGA-Au H-S NPs or HER-PLGA-Au H-S NPs at 37 °C for 24 h, and subjected them to TEM

[*] Dr. S.-M. Lee, H. Park, Prof. K.-H. Yoo
National Core Research Center for Nanomedical Technology
Yonsei University, Seoul 120-749 (Korea)
E-mail: khyoo@yonsei.ac.kr
Prof. K.-H. Yoo
Department of Physics, Yonsei University, Seoul 120-749 (Korea)
J.-W. Choi, Prof. C.-O. Yun
Graduate Program for Nanomedical Science
Yonsei University, Seoul 120-749 (Korea)
Prof. C.-O. Yun
Department of Bioengineering, Hanyang University, Seoul 133-791 (Korea)
Prof. Y. N. Park
Department of Pathology, Yonsei University College of Medicine
Seoul 120-749 (Korea)

[**] This work was financially supported by NRF through the National Core Research Center for Nanomedical Technology (Grant No. R15-2004-024-00000-0) and by Basic Science Research Program through the NRF funded by the Ministry of Education, Science and Technology (2010-0003946).

Supporting information for this article is available on the WWW under http://dx.doi.org/10.1002/anie.201101783.

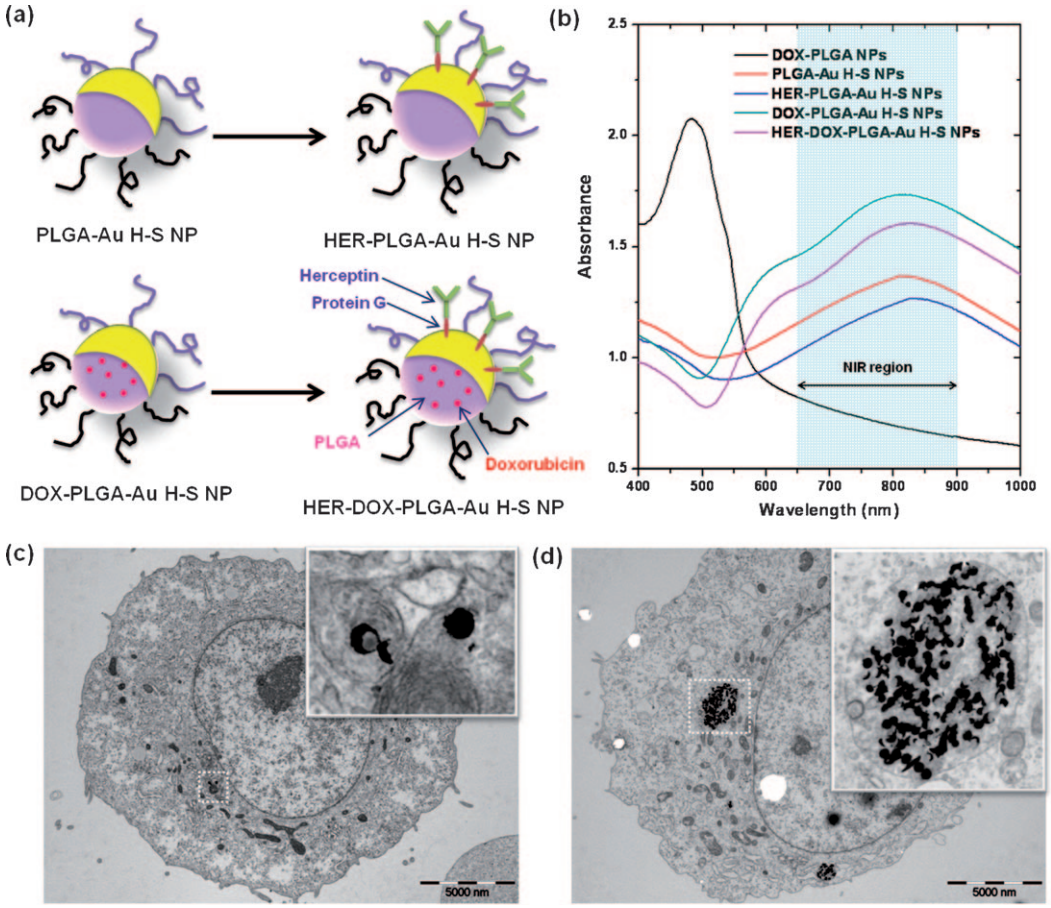

Figure 1. a) Schematic diagrams of PLGA-Au H-S NP, HER-PLGA-Au H-S NP, DOX-PLGA-Au H-S NP, and HER-DOX-PLGA-Au H-S NP. b) UV/Vis/NIR absorption spectra for DOX-PLGA NPs, PLGA-Au H-S NPs, HER-PLGA-Au H-S NPs, DOX-PLGA-Au H-S NPs, and HER-DOX-PLGA-Au H-S NPs. TEM images of SK-BR-3 cancer cells treated with PLGA-Au H-S NPs (c) and HER-PLGA-Au H-S NPs (d). The insets show enlarged TEM images taken from the area denoted by the rectangular boxes.

(Figure 1c and d). More nanoparticles were observed in the cells treated with HER-PLGA-Au H-S NPs than in the cells treated with PLGA-Au H-S NPs, and this implies that the HER-PLGA-Au H-S NPs were more easily internalized by the cells by receptor-mediated endocytosis than the PLGA-Au H-S NPs, which were likely internalized through pinocytosis. TEM images of SK-BR-3 cancer cells incubated with HER-PLGA-Au H-S NPs for different times are shown in Figure S1 of the Supporting Information. HER-PLGA-Au H-S NPs were found both inside and outside of vesicles, and this suggests that some NPs may escape from the vesicles.

To evaluate the in vivo targeting efficacy of HER-PLGA-Au H-S NPs, we prepared tumor-bearing mice by implanting SK-BR-3 cells into the dorsal subcutis of Balb/C nude mice. When the tumors reached approximately 100 mm^3 in size, we administered 200 μL of HER-PLGA-Au H-S NPs (1 $mg\,mL^{-1}$ dispersed in phosphate-buffered saline) to the mouse intravenously (IV) into the tail vein. The injected HER-PLGA-Au H-S NPs were monitored by measuring time-lapse in vivo NIR images with the eXplore Optix System (Figure 2a, top panels). The absorbance intensity changed in the tumor region 12 h after injection due to localization of HER-PLGA-Au H-S NPs in the tumor; in particular, a gradual change in absorbance intensity (from green to blue in Figure 2a, top panels) occurred in the middle of the tumor, indicating that HER-PLGA-Au H-S NPs accumulated in this region over time. We compared this effect with passive targeting by enhanced permeability and retention effect by performing similar experiments with the PLGA-Au H-S NPs (Figure 2a, bottom panels). Plotting the number of pixels with absorbance intensity $\geq 6.15 \times 10^3$ a.u. (blue in Figure 2a) revealed that their number increased up to 48 h after treatment, then slightly decreased (Figure 2b), probably due to slow release of NPs from the tumor site caused by leaky angiogenic vessels and poor lymphatic drainage. However, nearly twice as many high-absorbance pixels were found in the mouse treated with HER-PLGA-Au H-S NPs than in the mouse treated with PLGA-Au H-S NPs (Figure 2b), that is, NPs were more effectively delivered to the tumor through active targeting with HER-PLGA-Au H-S NPs than passive targeting with PLGA-Au H-S NPs. We also measured ex vivo NIR images of major organs (kidney, lung, and tumor tissue) excised 3 d post-injection (Figure S2, Supporting Information). Compared with PLGA-Au H-S NP-treated tumor tissue, stronger NIR absorption was found in the HER-PLGA-Au H-S NP-treated tumor tissue, that is, HER-PLGA-Au H-S NPs were more effectively delivered to the tumor.

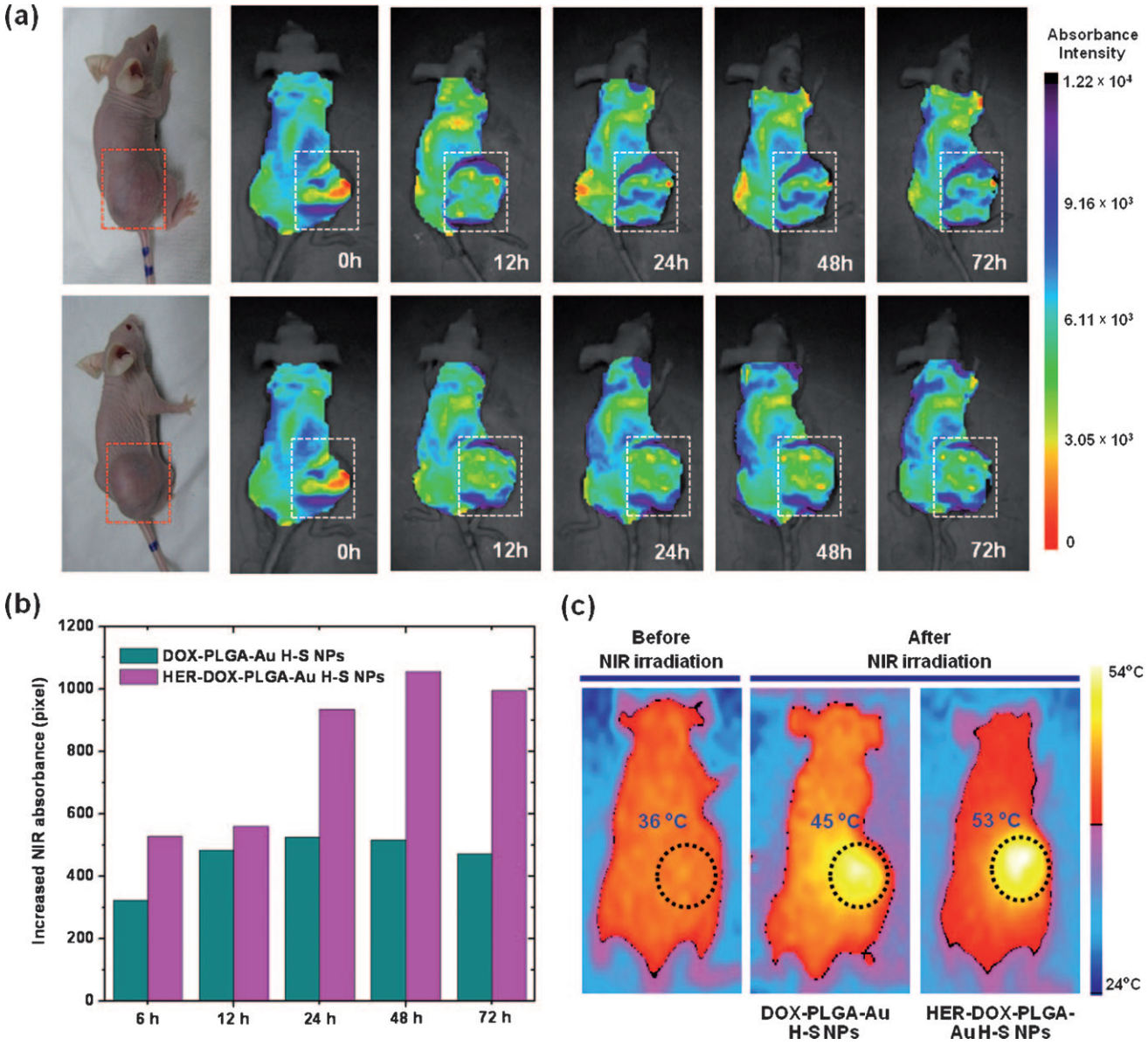

Figure 2. a) Time-lapse in vivo NIR images of SK-BR-3 tumor-bearing mouse after IV tail injection of HER-PLGA-Au H-S NPs (top panels) or PLGA-Au H-S NPs (bottom panels). b) The number of pixels in which the absorption intensity was above 6.15×10^3 a.u. as a function of time for the SK-BR-3 tumor-bearing mouse treated with HER-PLGA-Au H-S NPs or PLGA-Au H-S NPs. c) Thermal images of the SK-BR-3 tumor-bearing mouse treated with PLGA-Au H-S NPs or HER-PLGA-Au H-S NPs before and after the tumor region (diameter 1 cm) was exposed to 1.82 $W cm^{-2}$ NIR light for 10 min.

Heat is locally generated on NIR irradiation since the Au half-shells have an absorption peak in the NIR region. To determine the temperature increase following NIR exposure, we measured the temperature of the tumor tissue using a 24-gauge thermocouple needle (Brymill, Ellington, CT, USA) inserted beneath the tumor while the tumor region was exposed to 1.82 $W cm^{-2}$ NIR light for 10 min with a laser diode ($\lambda = 808$ nm, Figure S3 of the Supporting Information). The tumor temperature increased by approximately 20 and 30 °C for mice treated with PLGA-Au H-S NPs and HER-PLGA-Au H-S NPs at 24 h post-injection, respectively, temperature changes that are sufficient to induce irreversible tissue damage. Since higher concentrations of NIR-resonant NPs result in higher temperatures for the same NIR light power, our measurements indicate that more HER-PLGA-Au H-S NPs accumulated in the tumor by active targeting than did PLGA-Au H-S NPs by passive targeting.

We monitored mice treated with HER-DOX-PLGA-Au H-S NPs and DOX-PLGA-Au H-S NPs before and after NIR irradiation (Figure 2c) with a thermal imaging camera (AXT100, Ann Arbor Sensor Systems). Before NIR exposure, the temperature of the tumor tissue of about 36 °C corresponded to the body temperature of the mouse. However, after the tumor region (diameter 1 cm) was exposed to 1.82 $W cm^{-2}$ NIR light for 10 min with a laser diode ($\lambda =$ 808 nm), the tumor temperature increased up to 45 and 53 °C for mice treated with DOX-PLGA-Au H-S NPs and HER-DOX-PLGA-Au H-S NPs for 24 h, respectively. Mean-

while, the regions not exposed to NIR light experienced a lesser increase in temperature (Figure S4, Supporting Information). These observations confirm that heat can be delivered to only the tumor region with a laser-guided light source.

We carried out comparative studies on the therapeutic efficacies of chemophotothermal treatments combined with targeted delivery. We divided the SK-BR-3 tumor-bearing mice into seven groups ($n = 3$ mice per group). When the tumors developed to approximately 100 mm^3, 200 μL of each treatment were administered by IV tail injection (Table 1). The relative tumor volumes were measured for each group and plotted as a function of time (Figure 3a); the relative volume was defined as $(V-V_0)/V_0$ (V_0: initial tumor volume).

Table 1: Summary of treatments applied to mice for comparative study of therapeutic efficacy.

Group	Administered content[a]	Dosage of DOX [$mg\,kg^{-1}$]	Dosage of HER [$mg\,kg^{-1}$]	NIR light[b] [$W\,cm^{-2}$]
1	saline	–	–	–
2	free DOX	10	–	–
3	free HER	–	16	–
4	HER-DOX-PLGA-Au H-S NPs	0.18	0.58	–
5	HER-PLGA-Au H-S NPs	–	0.64	1.82
6	DOX-PLGA-Au H-S NPs	0.25	–	1.82
7	HER-DOX-PLGA-Au H-S NPs	0.18	0.58	1.82

[a] Administrated content was injected intravenously by tail vein in a volume of 200 μL with a concentration of nanoparticles of 1 $mg\,mL^{-1}$. [b] The tumor was exposed to NIR light for 10 min with a laser diode ($\lambda = 808$ nm) at 24 h post-injection of nanoparticles.

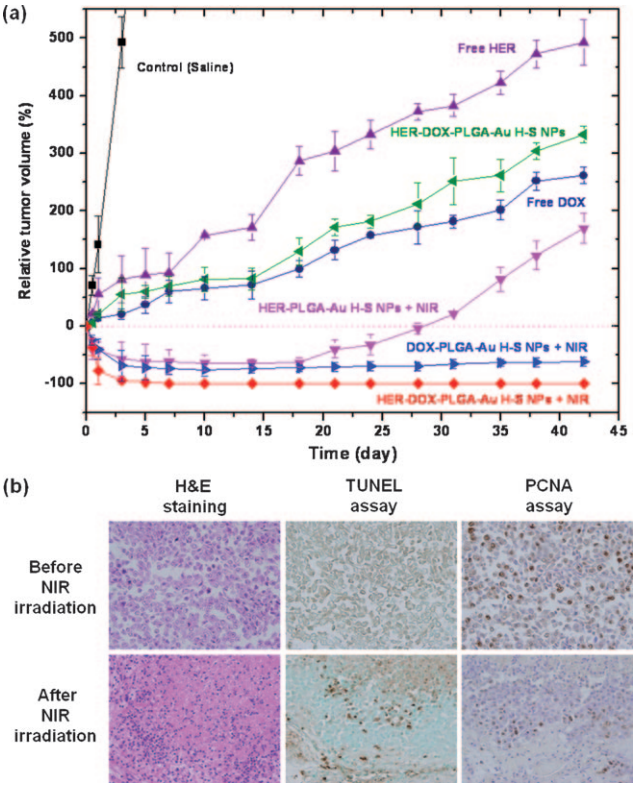

Figure 3. a) Relative change in tumor volume versus time for mice treated with saline (■), free DOX (●), free HER (▲), HER-DOX-PLGA-Au H-S NPs (◀), HER-PLGA-Au H-S NPs and NIR light (▼), DOX-PLGA-Au H-S NPs and NIR light (▶), or HER-DOX-PLGA-Au H-S NPs and NIR light (◆). b) Histology of the tumor tissue collected at 5 d after injection of saline (top panel) or HER-DOX-PLGA-Au H-S NPs (bottom panel) followed by NIR irradiation. Images were acquired at 400× magnification.

When the mice were treated with DOX alone ($10\,mg\,kg^{-1}$), HER ($16\,mg\,kg^{-1}$), or HER-DOX-PLGA-Au H-S NPs without NIR irradiation ($0.18\,mg\,kg^{-1}$ for DOX), the tumor volumes increased continuously, although the growth rates were much lower than that of the control group (Figure 3a). We interpreted these results to mean that the injected dosage of DOX or HER was too low to inhibit tumor growth. Treatment with HER-DOX-PLGA-Au H-S NPs yielded similar effects to treatment with free DOX despite different DOX dosages (0.18 and $10\,mg\,kg^{-1}$), an observation we ascribe to accumulation of HER-DOX-PLGA-Au H-S NPs by active targeting and/or to the therapeutic effects of HER as well as DOX.

On the other hand, when the mice were treated with HER-PLGA-Au H-S NPs, DOX-PLGA-Au H-S NPs ($0.25\,mg\,kg^{-1}$ of DOX), or HER-DOX-PLGA-Au H-S NPs ($0.18\,mg\,kg^{-1}$ of DOX) and then exposed to $1.82\,W\,cm^{-2}$ NIR light for 10 min, all mice exhibited substantial decreases in tumor volume, dependent on the treatment type (Figure 3a). The volumes of tumors treated with HER-PLGA-Au H-S NPs decreased by about 65% over 18 d, after which the tumor began to grow again rapidly. Tumor recurrence was attributed to incomplete destruction of tumor tissue; heat sufficient to destroy the tumor tissue completely was not delivered to the tumor due to the low power of the NIR light or the low concentration of HER-PLGA-Au H-S NPs localized in the tumor region. The mice that were treated with DOX-PLGA-Au H-S NPs and exposed to NIR light experienced tumor reductions of 75% in 10 d. However, incomplete tumor destruction caused the tumor volume to increase after 10 d (Figure S5, Supporting Information), although the growth rate of the tumor was very low, probably due to DOX cytotoxicity. Finally, when mice were treated with HER-DOX-PLGA-Au H-S NPs and exposed to NIR light, the tumors were completely destroyed 7 d after NIR irradiation, and no tumor recurrence was observed for 42 d (Figure S6, Supporting Information). Taken together, these observations demonstrate that chemophotothermal treatment with active targeting provides higher therapeutic efficacy with a lower DOX dosage than chemophotothermal treatment with passive targeting. Although lower dosages of HER-DOX-PLGA-Au H-S NPs were injected than DOX-PLGA-Au H-S NPs, more HER-DOX-PLGA-Au H-S NPs accumulated in the tumor through active targeting, and consequently, more DOX, heat, and HER were delivered to the tumors, resulting in higher therapeutic efficacy.

To confirm the effect of the chemophotothermal treatment, we performed histological examinations of tumor tissues 5 d after IV injection of HER-DOX-PLGA-Au H-S NPs and NIR irradiation (Figure 3b). After NIR irradiation,

marked thermonecrosis developed, and apoptotic cells were also frequently identified by terminal deoxynucleotidyl transferase dUTP nick end labeling (TUNEL), and the proliferating cell nuclear antigen (PCNA) assay showed that most cells were unable to proliferate following chemophotothermal treatment.

An important concern for nanoparticle-based treatments is whether the injected nanoparticles accumulate in organs or are cleared from the body. To investigate the organ distribution and tumor uptake of HER-DOX-PLGA-Au H-S NPs, we measured the accumulated Au in major organs and tumors at 1, 5, and 42 d after IV injection using an inductively coupled plasma mass spectrometer (Figure 4a). One day post-injection, 2.9 μg of Au was found in the tumor tissue, corresponding to about 10% of the injected HER-DOX-PLGA-Au H-S NPs, an amount larger than the 3.5% measured following injection of DOX-PLGA-Au H-S NPs. These results confirm that a greater amount of HER-DOX-PLGA-Au H-S NPs than DOX-PLGA-Au H-S NPs accumulated in the tumor site due to targeted delivery of conjugated HER to the overexpressed HER2 receptors of the SK-BR-3 cells in the mouse. The HER-DOX-PLGA-Au H-S NPs were also efficiently taken up by the reticuloendothelial organs, such as the liver and spleen, with lesser accumulation in the kidney, lung, or heart. However, most HER-DOX-PLGA-Au H-S NPs were cleared from the body after 42 d (Figure 4a).

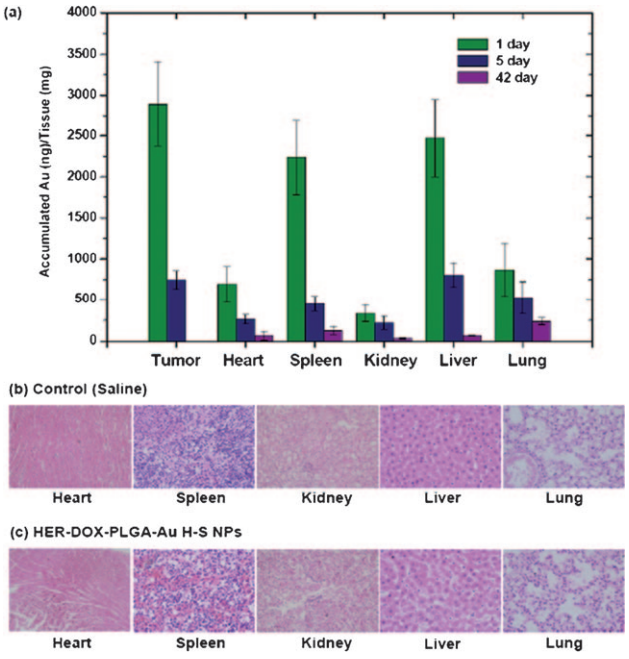

Figure 4. a) Tissue distribution of NPs in major organs at different times. Tissue distributions of Au in HER-DOX-PLGA-Au H-S NPs were measured by inductively coupled plasma mass spectroscopy ($n = 3$ per group). Histological sections of major organs (heart, spleen, kidney, liver, and lung) were collected 5 d after injection of saline (b) or HER-DOX-PLGA-Au H-S NPs (c) followed by NIR irradiation. Images were acquired at 400× magnification.

Since HER-DOX-PLGA-Au H-S NPs were taken up by organs as well as the tumor, we carried out histological examinations of major organs to investigate the normal tissue toxicity caused by HER-DOX-PLGA-Au H-S NPs 5 d after IV injection of HER-DOX-PLGA-Au H-S NPs and NIR irradiation (Figure 4b). No tissue damage was evident in comparison with the NP-free control, and this implies that HER-DOX-PLGA-Au H-S NPs that accumulated in other organs did not induce in vivo toxicity. We further examined liver toxicity by measuring interleukin-6 (IL-6), aspartate aminotransferase (AST), and alanine aminotransferase (ALT) in blood (Table S1, Supporting Information). Similar values were found for NP-free control mice and the mice treated with HER-DOX-PLGA-Au H-S NPs and exposed to NIR light, that is, HER-DOX-PLGA-Au H-S NPs caused no liver toxicity.[6] In addition, we measured body weight during the treatments, since high toxicity usually results in weight loss. The absence of weight loss in any treatment group (Figure S7, Supporting Information) implies that the toxicity of the treatments was not severe.

In summary, we have developed HER-DOX-PLGA-Au H-S NPs that can carry heat and drugs specifically to tumors through active targeting, and investigated the therapeutic efficacy of these multifunctional NPs in SK-BR-3 tumor-bearing mice. In vivo NIR images revealed that the NPs are more effectively delivered to the tumor by active targeting with HER-DOX-PLGA-Au H-S NPs than by passive targeting with DOX-PLGA-Au H-S NPs. On NIR irradiation (1.82 W cm^{-2} for 10 min) a higher intratumoral temperature was measured for the mouse treated with HER-DOX-PLGA-Au H-S NPs, that is, more heat, drug, and HER could be delivered to the tumor tissue by active targeting. Chemophotothermal treatment combined with targeted delivery resulted in complete tumor destruction without recurrence with only 0.18 mg kg^{-1} of DOX and 1.82 W cm^{-2} NIR light. However, the tumor was not completely destroyed and recurred following chemophotothermal treatment without targeted delivery, and after targeted drug delivery without NIR irradiation, although the same DOX dosage and NIR light power were applied. Taken together, these results demonstrate the excellent synergistic effects of targeted chemophotothermal treatments based on HER-DOX-PLGA-Au H-S NPs.

Received: March 12, 2011
Published online: June 30, 2011

Keywords: cancer · chemophotothermal treatment · drug delivery · nanoparticles

[1] a) K. Riehemann, S. W. Schneider, T. A. Luger, B. Godin, M. Ferrari, H. Fuchs, *Angew. Chem.* **2009**, *121*, 886–913; *Angew. Chem. Int. Ed.* **2009**, *48*, 872–897; b) O. C. Farokhzad, R. Langer, *ACS Nano* **2009**, *3*, 16–20; c) J. D. Byrne, T. Betancourt, L. Brannon-Peppas, *Adv. Drug Delivery Rev.* **2008**, *60*, 1615–1626; d) M. Wang, M. Thanou, *Pharm. Res.* **2010**, *62*, 90–99.

[2] a) G. M. Hahn, J. Braun, I. Har-Kedar, *Proc. Natl. Acad. Sci. USA* **1975**, *72*, 937–940; b) J. Overgaard, *Cancer Res.* **1976**, *36*, 3077–3081; c) H. A. Johnson, *J. Natl. Cancer Inst.* **1973**, *50*, 903–908; d) R. D. Issels, *Eur. J. Cancer* **2008**, *44*, 2546–2554.

[3] a) T. S. Hauck, T. L Jennings, T. Yatsenko, J. C. Kumaradas, W. C. W. Chan, *Adv. Mater.* **2008**, *20*, 3832 – 3838.
[4] a) H. Park, J. Yang, S. Seo, K. Kim, J. Suk, D. Kim, S. Haam, K. H. Yoo, *Small* **2008**, *4*, 192 – 196; b) H. Park, J. Yang, J. Lee, S. Haam, I. H. Choi, K. H. Yoo, *ACS Nano* **2009**, *3*, 2919 – 2926; c) S. M. Lee, H. Park, K. H. Yoo, *Adv. Mater.* **2010**, *22*, 4049 – 4053.
[5] a) S. C. Wuang, K. G. Neoh, E. T. Kang, D. W. Pack, D. E. Leckband, *Biomaterials* **2008**, *29*, 2270 – 2279; b) J. Yang, C.-H. Lee, H.-J. Ko, J.-S. Suh, H.-G. Yoon, K. Lee, Y.-M. Huh, S. Haam, *Angew. Chem. Int. Ed.* **2007**, *46*, 8836 – 8839.
[6] W. Lu, A. Huang, G. Ku, Z. Wen, M. Zhou, D. Guzaov, P. Brecht, R. Su, A. Oraevsky, L. V. Wang, C. Li, *Biomaterials* **2010**, *31*, 2617 – 2626.

